Research Article

XPS and GDOES Characterization of Porous Coating Enriched with Copper and Calcium Obtained on Tantalum via Plasma Electrolytic Oxidation

Krzysztof Rokosz,[1] Tadeusz Hryniewicz,[1] Patrick Chapon,[2] Steinar Raaen,[3] and Hugo Ricardo Zschommler Sandim[4]

[1]*Division of Bioengineering and Surface Electrochemistry, Department of Engineering and Informatics Systems, Faculty of Mechanical Engineering, Koszalin University of Technology, Racławicka 15-17, 75-620 Koszalin, Poland*
[2]*HORIBA Jobin Yvon S.A.S., 16-18 rue du Canal, 91165 Longjumeau Cedex, France*
[3]*Department of Physics, Norwegian University of Science and Technology (NTNU), Realfagbygget E3-124 Høgskoleringen 5, 7491 Trondheim, Norway*
[4]*Department of Materials Engineering, Lorena School of Engineering, University of Sao Paulo, 12602-810 Lorena, SP, Brazil*

Correspondence should be addressed to Tadeusz Hryniewicz; tadeusz.hryniewicz@tu.koszalin.pl

XPS and GDOES characterizations of porous coatings on tantalum after Plasma Electrolytic Oxidation (PEO) at 450 V for 3 minutes in electrolyte containing concentrated (85%) phosphoric acid with calcium nitrate and copper (II) nitrate are described. Based on the obtained data, it may be concluded that the PEO coating consists of tantalum (Ta^{5+}), calcium (Ca^{2+}), copper (Cu^{2+} and Cu^+), and phosphates (PO_4^{3-}). It has to be pointed out that copper and calcium are distributed throughout the volume. The authors also propose a new model of PEO, based on the derivative of GDOES signals with sputtering time.

1. Introduction

Tantalum, which was discovered by the Swedish chemist and mineralogist Anders Gustaf Ekeberg in 1802, is a transition metal of grayish-silver color with atomic number and atomic mass equal to 73 and 180.9479, respectively. It is very hard, malleable, and ductile and has excellent corrosion resistance to acids and other strong chemicals. Therefore it is used *inter alia* in chemical, metallurgy, textile, aerospace, medical, dental, electronic, and optic industries. In case of biomedical applications it is used for surgical clips, bone grafts, and plates for cranioplasty as well as mesh for abdominal wall reconstruction and dental implants [1]. Tantalum [2–5] as well as niobium [6–9], zirconium [10–13], and titanium [14–17] and its alloys [18–24] may be treated by Plasma Electrolytic Oxidation method, known also worldwide as Micro Arc Oxidation to form porous coating containing chemical compounds dissolved in a solution. The results presented in

paper are the first ones and in our opinion interesting for other researchers; in near future we will present the new ones, which will be obtained in electrolytes based on different concentrations of $Cu(NO_3)_2$ and $Ca(NO_3)_2$ in H_3PO_4. In addition, it is beneficial to also enrich the porous coatings with antibacterial agent such as copper [25–32] to speed up wound healing and reduce the risk of infection after surgery.

In the present paper, authors described the porous coating obtained on Ta surface and featuring copper and calcium enrichment in its volume. XPS and GDOES techniques allowed characterizing the in-depth composition and description of the chemical compounds of the obtained PEO coating.

2. Method

2.1. Material. A set of tantalum samples with Plasma Electrolytic Oxidation (Micro Arc Oxidation) served for the

study. The samples (from same original material) were cut in the shape of cylindrical specimens of diameter 10 mm with a height of 5 mm. The round top surface of the samples was mechanically polished using SiC abrasive paper with grain of 1000-grit size.

2.2. Set-Up and Parameters. The Plasma Electrolytic Oxidation (PEO) was performed at the DC voltage of 450 ± 10 V during 3 minutes of treatment. The studies were carried out with an electrolyte of initial temperature of $20 \pm 2°C$. For these studies, the electrolyte was composed of 300 g $Cu(NO_3)_2$ and 300 g $Ca(NO_3)_2$ in 1 liter of concentrated orthophosphoric acid (85% H_3PO_4). For each run, an electrolytic cell made of glass was used, containing up to 500 ml of the electrolyte. At the beginning the one liter of orthophosphoric acid was warmed up to about 70°C and the two salts were added. After that the salts were mixed for the time of 6 hours. In that case the colloid, not a solution, was obtained. It has to be also pointed out that just after preparing the electrolyte was used.

2.3. SEM and XPS Studies. The scanning electron microscope Quanta 250 FEI with Low Vacuum and ESEM mode and a field emission cathode to obtaining images of top surface of tantalum after Plasma Electrolytic Oxidation was used. The X-ray Photoelectron Spectroscopy (XPS) measurements on tantalum samples were performed on a SCIENCE SES 2002 instrument using a monochromatic (Gammadata-Scienta) Al K(alpha) ($h\nu$ = 1486.6 eV) X-ray source (18.7 mA, 13.02 kV). Scans analyses were carried out with an analysis area of 1 × 3 mm and a pass energy of 500 eV with the energy step 0.2 eV and step time 200 ms. The binding energy of the spectrometer has been calibrated by the position of the Fermi level on a clean metallic sample. The power supplies were stable and of high accuracy. The experiments were carried out in an ultra-high-vacuum system with a base pressure of about $6 \cdot 10^{-8}$ Pa. The power of the X-ray source was given as follows: 18.7 mA × 13.02 kV = 243.5 W. The pass energy of 500 eV gives an energy resolution of near 1 eV. This high pass energy was chosen to improve the signal to noise ratio in the photoemission spectra. The XPS spectra were recorded in normal emission. For the XPS analyses the CasaXPS 2.3.14 software (Shirley background type) [33] with the help of XPS tables [28] was used. All the binding energy values presented in that paper were charge corrected to C 1s at 284.8 eV. The number of sweeps during the XPS measurements was different for each element, because of different noisiness and amplitude of those signals. Hence, because of strong signals for carbon (C 1s), oxygen (O 1s), and calcium, only 9 sweeps (signal/noise = 3) were performed. In case of P and Ta, for phosphorus (P 2p) and tantalum (Ta 4f, Ta 4d), 16 (signal/noise = 4) and 64 sweeps (signal/noise = 8), respectively, were used. For very weak signals of copper (Cu 2p, Cu LMM), 225 sweeps were done giving a signal to noise ratio (S/N) equaling 15. In case of the two XPS survey spectra, only 1 sweep for each one was performed.

2.4. GDOES Studies. The Glow Discharge Optical Emission Spectroscopy (GDOES) measurements on PEO oxidized tantalum samples were performed on a Horiba Scientific
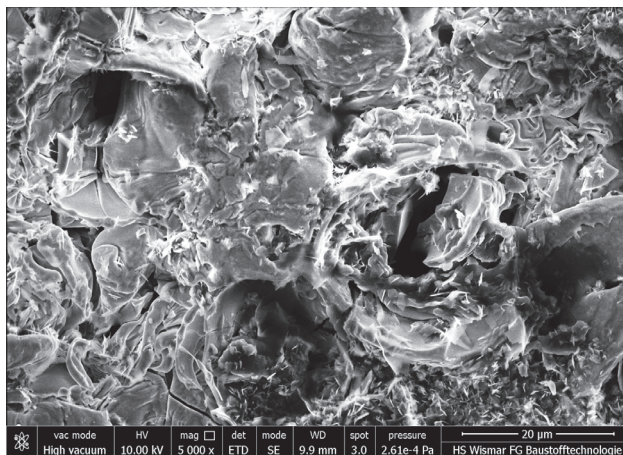

Figure 1: SEM image of tantalum surface after PEO treatment at 450 V in electrolyte containing $Ca(NO_3)_2$ and $Cu(NO_3)_2$.

GD Profiler 2 instrument using radio frequency (RF) asynchronous pulse generator with the following conditions: pressure: 700 Pa, power: 40 W, frequency: 3000 Hz, duty cycle: 0.25, and anode diameter: 4 mm. The signals of copper (325 nm), phosphorus (178 nm), oxygen (130 nm), nitrogen (149 nm), hydrogen (122 nm), and tantalum (301 nm) were measured [34].

3. Results and Discussion

In Figure 1, the SEM image is presented. The observed surface of tantalum after plasma electrolytic treatment is not so porous as it was observed on titanium and its alloys. However, the obtained PEO coating is not as flat as after electrochemical polishing and may be used in production of promoters for catalysts or as biomaterial.

In Figures 2 and 3, survey and XPS spectra, respectively, are shown. It has to be noted that, to understand the chemical composition of the top layer (top 10 nm) of PEO coating, the XPS measurements are necessary. Based on the information from Figure 2 spectra one may note that oxygen (O 1s, O KLL), carbon (C 1s), phosphorus (P 2s, P 2p), calcium (Ca 2p, Ca 3p, Ca 3s), copper (Cu 2p), and tantalum (Ta 4f, Ta 4d, Ta 5s, Ta 5p) were found out. Because the copper (Cu 2p) signal was very weak, the Auger copper peak (Cu $L_3M_{4,5}M_{4,5}$) was not visible after 1 sweep survey scan.

In order to find the oxidation states of all elements and to calculate the chemical composition of the top 10 nm of the PEO coating, it was necessary to perform XPS high-resolution studies. The results of those high-resolution XPS measurements are demonstrated in Figure 3. Carbon, which most probably originates from the purification process (C_2H_5OH) and the atmosphere (CO_2), should be treated as a contamination. However, it is necessary for the calibration process of all spectra (the signal of C–C/C–H bonding must be set at 284.8 eV) and because of interpretation process, with the use of data from reference XPS bases. On the basis of information from Figure 3, it can be stated that the top 10 nm of PEO coating consists of phosphates of tantalum and/or
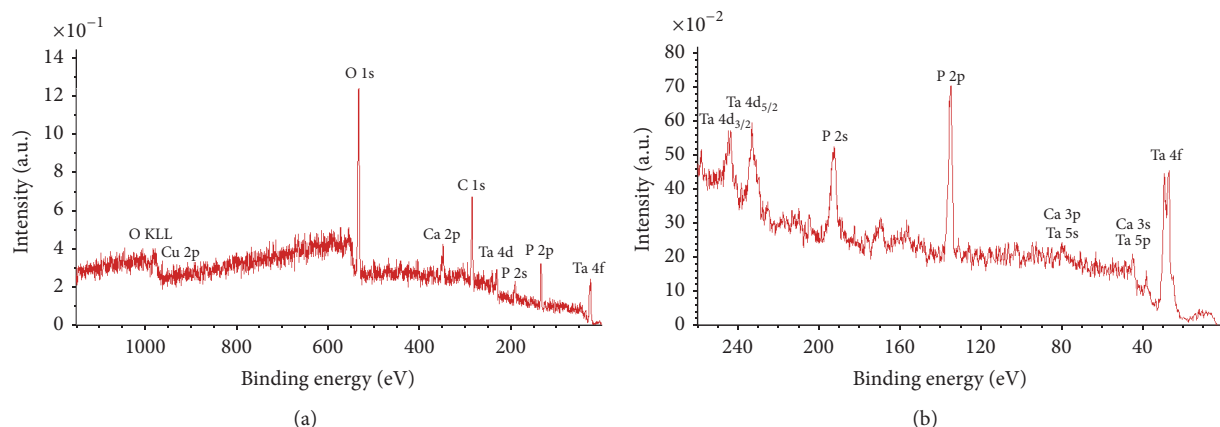
FIGURE 2: XPS survey spectra of top 10 nm of tantalum surface after PEO treatment at 450 V in electrolyte containing $Ca(NO_3)_2$ and $Cu(NO_3)_2$, with maximum binding energy 1150 eV (a) and 260 eV (b).
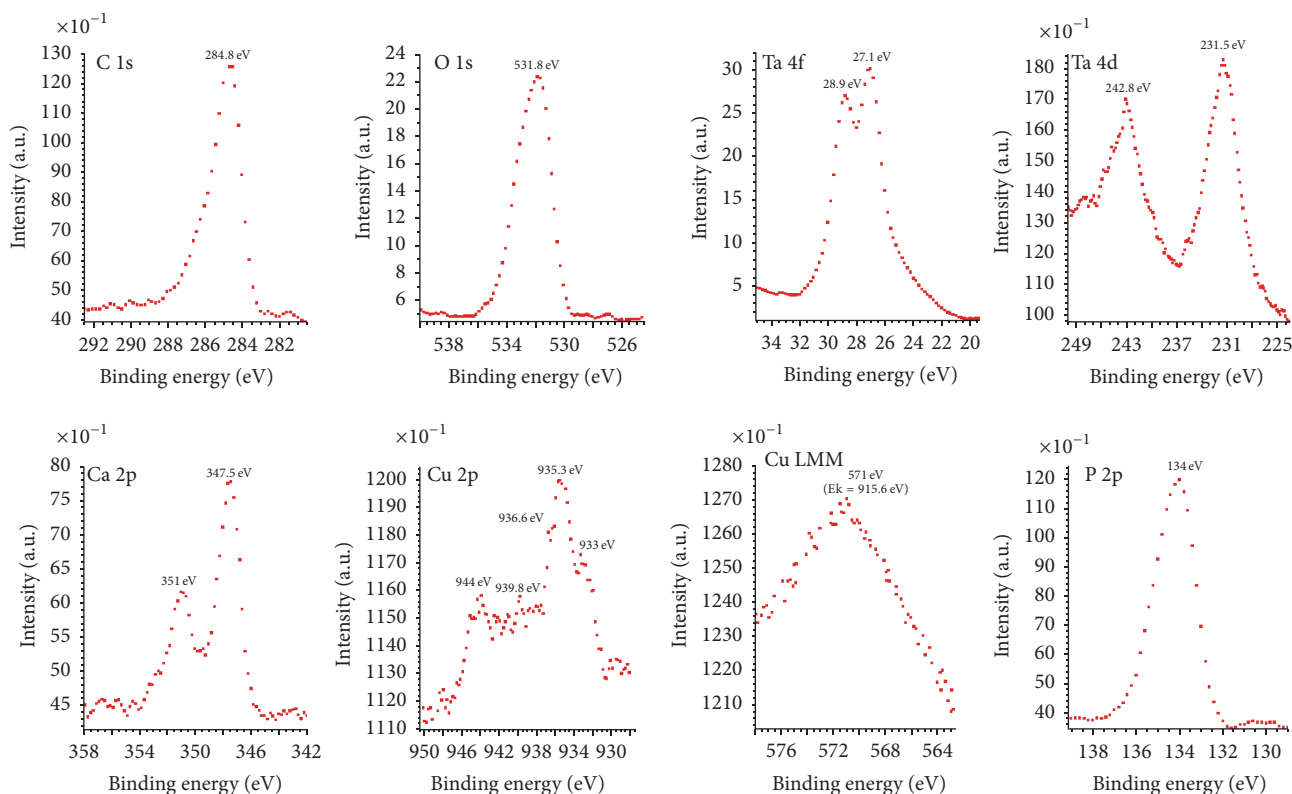

FIGURE 3: XPS spectra of carbon (C 1s), oxygen (O 1s), tantalum (Ta 4f, Ta 3d), calcium (Ca 2p), copper (Cu 2p, Cu LMM), and phosphorus (P 2p).

calcium and copper, the binding energy for phosphorus (P 2p) is 134 eV, and that of oxygen (O 1s) is 513.8 eV. The binding energy of calcium (Ca 2p), which equals 347.5 eV, suggests that calcium is on the second stage of oxidation (Ca^{2+}) and occurs most likely as $CaHPO_4$ and/or $Ca_3(PO_4)_2$ [27, 28]. In order to find the oxidation stages of copper as well as differentiate Cu^0 from Cu^+ and Cu^{2+}, the regions of the spectra, that is, Cu 2p and Cu $L_3M_{4,5}M_{4,5}$ [29–33], have to be studied. Based on binding energies of Cu 2p spectra and

their modified Auger parameters (MAP), which are equal to 935.3 eV (MAP = 1850.9 eV) and 936.6 eV (MAP = 1851.6 eV), and their satellites with binding energies equaling 939.8 eV and 944 eV, it is possible to state surely that copper is on the second stage of oxidation (Cu^{2+}). However, the Cu 2p binding energy equaling 933 eV with the modified Auger parameter amounting to 1848.6 eV corresponds to Cu^+.

The spectrum of Ta 4f binding energy region may be deconvoluted into two peaks, which are centered at 27.1 eV (Ta

Table 1: Total chemical composition of coating formed after PEO treatment at 450 V on tantalum with outer carbon- and biocontaminations sublayer at% (based on XPS results).

Tantalum	Calcium	Copper	Phosphorus	Oxygen	Carbon
1.1	4.6	0.3	17.7	37.7	38.6

Table 2: Total chemical composition of coating formed after PEO treatment at 450 V on tantalum without outer carbon- and biocontaminations sublayer at% (based on XPS results).

Tantalum	Calcium	Copper	Phosphorus
4.8	19.4	1.3	74.5

$4f_{7/2}$) and 28.9 eV (Ta $4f_{5/2}$), which may suggest that tantalum is on the fifth stage of oxidation (Ta^{5+}).

Based on this information, from XPS data, complex formulae should contain tantalum, calcium, and copper phosphates which may be representative for the studied PEO coating.

In Tables 1 and 2, the chemical compositions of PEO layer are presented, wherein in the first one are presented results containing outer carbon- and biocontaminations sublayer. Table 2 contains calculated values without oxygen (O 1s) and carbon (C 1s). Based on these data, it is possible to conclude that the top 10 nm layer of PEO coating consists mainly of calcium phosphates with some tantalum and/or copper phosphates. It is a very good result because the human bone is containing mainly hydroxyapatite, which consists generally of Ca^{2+} and PO$_4$$^{3-}$. The additional doping with copper provides additional antibacterial properties for the coating that is necessary because of high amount of microbes in live organism during surgery. It has to be pointed out that Cu^{2+} ions, normally located within hydroxyapatite- (HA-) structure [Ca$_5$(PO$_4$)$_3$(OH) or Ca$_{10}$(PO$_4$)$_6$(OH)$_2$], are randomly substituted (or superimposed) by Cu^{2+} [35] coming from the electrolyte.

In Figure 4, the GDOES depth profile results of tantalum, phosphorus, oxygen, copper, calcium, hydrogen, and nitrogen on one graph, are shown. Important is to remember that the curves presented in Figure 3 are not in atomic nor weight percentage but only show the relative light intensities of GDOES signals multiplied by 10, 1.5, 1, 1.5, 1.5, 1.13, and 7 for hydrogen, nitrogen, oxygen, calcium, phosphorus, tantalum, and copper, respectively (qualitative depth profiles). By the same token the x-axis displays the erosion time and not directly the depth (as it is difficult to precisely estimate rough, porous materials).

The signals were scaled on the model describing the coating obtained on tantalum by PEO. From these GDOES signals, it is possible to find out three sublayers. The first-top one (0–40 s by sputtering time) is containing the smallest amount of tantalum and calcium and the highest amount of phosphorus, copper, oxygen, nitrogen, and hydrogen. The second one (40–80 s by sputtering time) is semiporous and enriched in calcium, copper, and oxygen. The next sublayer, transition one (80–300 s by sputtering time), has local maxima of phosphorus and hydrogen, which maybe
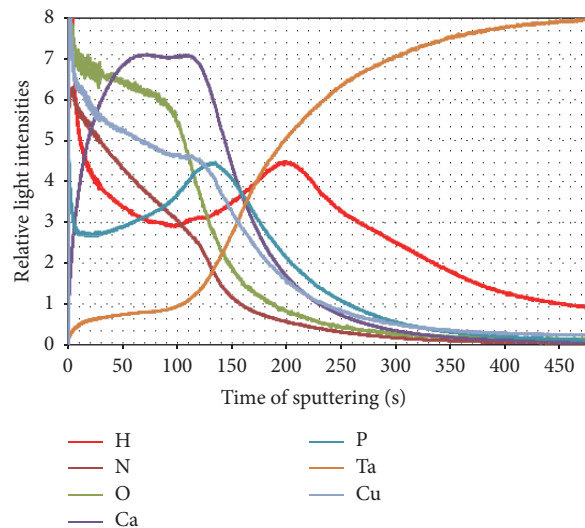

Figure 4: Relative light intensities of tantalum, phosphorus, calcium, copper, oxygen, and nitrogen of PEO coating formed on tantalum obtained by GDOES method. The first 20 s was recorded with higher acquisition frequency and no smoothing with equal spacing was applied; this is why the further derivatives look more noisy in this first part.

reveal the presence of molecules of water or phosphoric acid inside that sublayer.

To find out all the sublayers, based on Figure 4, the derivatives by sputtering time of the GDOES signals were calculated and are presented in Figure 5, for phosphorus, copper, oxygen, nitrogen, tantalum, and calcium along with their derivatives, respectively. Based on that mathematical analysis of these signals, it was possible to find the three sublayers: the first-top one (from 0 till about 40 s), the second one (from about 40 s till about 80 s), and the third one (from about 80 s till about 300 s). The last sublayer, which is deeper than 300 s of sputtering process, is a transition layer, in which all signals of electrolyte elements, that is, phosphorus, calcium, copper, oxygen, and nitrogen, are decreasing and the tantalum signal is the only increasing one up to the matrix level. A decreasing of oxygen and nitrogen may be found for depths related to sputtering times from 80 s till 300 s that should be recognized as a transition zone. However, it has to be noted that the derivatives of oxygen and nitrogen signals have the same inflection points, that is, about 125 s, what may suggest that distribution of these elements in the sublayer takes place along two different curves; that is, that the sublayer may be divided into two additional parts, where the second one is thicker and less enriched in oxygen and nitrogen than the first one. Based on the oxygen and nitrogen GDOES signals and their derivatives, it can be stated that an additional sublayer boundary may be determined by the inflection points of these two curves. Similar information can be taken out from the copper and calcium signals and their derivatives. In case of copper, two regions are visible, that is, an enriched one, observed from the top to depth related to sputtering time that equals 150 s, and a depleted zone for deeper layers. The calcium signal at the top sublayer was small and reached the
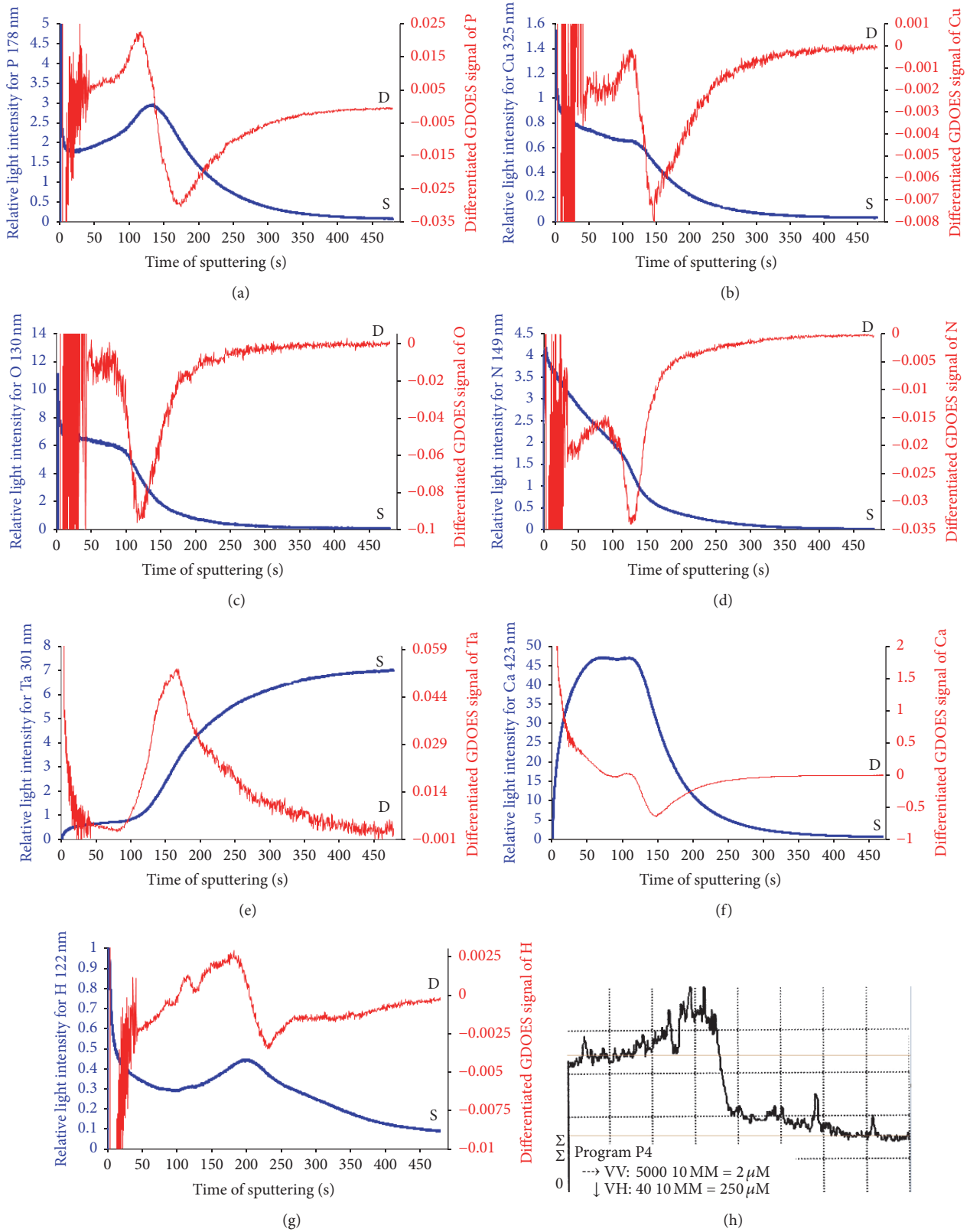
Figure 5: GDOES signals (S) of (a) phosphorus, (b) copper, (b) oxygen, (d) nitrogen, (e) tantalum, (f) calcium, and (g) hydrogen (blue lines) and their derivatives (D) (red lines) as well as (h) a GDOES crater's portion of coating formed on tantalum. (Cf. comment of Figure 3, smoothing with equaling spacing will allow "removing" the noise at the beginning.)

maximum values in the second sublayer, that is, for sputtering times from 40 s till 150 s. However, the inflection point of declining slopes of the curves has value of about 150 s and it is dividing the third sublayer into the two additional parts, that is, with and without copper and calcium enrichment. The part of PEO coating enriched in hydrogen can be found in the depth related to sputtering time in the range of 125–270 s, which is confirmed by the analysis of derivative signal of hydrogen. Based on that analysis, additionally, the local maximum of differential of hydrogen signal for about 115 s may be found out: it corresponds to maximum of copper differential signal and maximum in differential signal of phosphorus.

Following the obtained GDOES results, it may be concluded that measured sputtering times related to depths of sublayers' boundaries are not only 40 s, 80 s, and 300 s, as it was found on the basis of Figure 4, but also 125 s, 150 s, and 270 s, what has been confirmed by the derivatives of the GDOES signals presented in Figure 5. The top layer, located in the sputtering time range of 0–40 s, is containing the minimum amounts of tantalum and calcium and the highest amounts of phosphorus, copper, oxygen, nitrogen, and hydrogen. The second one, which is located in the sputtering time range of 40–80 s, is semiporous and enriched in calcium, copper, and oxygen. The third one (80–300 s) consists of a local maxima of phosphorus as well as of hydrogen, what may be interpreted as molecules of water or phosphoric acid inside that sublayer. Moreover, that layer consists of four zones.

The fist zone appears to be for the sputtering time 80–125 s, with the enrichment of calcium, copper, and oxygen signals and depletion of tantalum and hydrogen ones. In that zone, the increase of phosphorus and decrease of nitrogen signals are recorded. In the second zone (125–150 s), the maximum of phosphorus signal is noted as well as increase of tantalum and hydrogen signals and decrease of calcium, copper, oxygen, and nitrogen ones. In the next zone, that referred to the sputtering time between 150 s and 270 s, a maximum of hydrogen signal was recorded. In addition, the signals of calcium, copper, phosphorus, oxygen, and nitrogen have a decreasing trend, while the tantalum one has got a growing trend. The last zone of the third sublayer, related to the sputtering time equaling 270–300 s, includes an area in which all the signals have decreased, except that of tantalum.

4. Conclusion

Based on the XPS results, it has to be stated that PEO coating on Ta consists mainly of tantalum phosphate with some amount of calcium and/or copper phosphates. The tantalum (Ta^{5+}), calcium (Ca^{2+}), copper (Cu^{+} and Cu^{2+}), and phosphorus (PO_4^{3-}) were found out in the top layer of PEO coating. Hence, most likely the complex formulae contain tantalum, calcium, and copper phosphates, to describe the chemical compounds of the obtained PEO coating.

Competing Interests

The authors declare that there is no conflict of interests regarding the publication of this paper.

References

[1] T. Espinoza, "Case study: tantalum in the world economy: history, uses and demand," POLINARES Consortium, Grant Agreement 224516, 2012.

[2] M. Sowa, A. Kazek-Kęsik, R. P. Socha, G. Dercz, J. Michalska, and W. Simka, "Modification of tantalum surface via plasma electrolytic oxidation in silicate solutions," *Electrochimica Acta*, vol. 114, pp. 627–636, 2013.

[3] C. C. Wang, F. Wang, and Y. Han, "The structure, bond strength and apatite-inducing ability of micro-arc oxidized tantalum and their response to annealing," *Applied Surface Science*, vol. 361, pp. 190–198, 2016.

[4] M. Petković, S. Stojadinović, R. Vasilić, I. Belča, B. Kasalica, and L. Zeković, "Plasma electrolytic oxidation of tantalum," *Serbian Journal of Electrical Engineering*, vol. 9, no. 1, pp. 81–94, 2012.

[5] M. Petković, S. Stojadinović, R. Vasilić, and L. Zeković, "Characterization of oxide coatings formed on tantalum by plasma electrolytic oxidation in 12-tungstosilicic acid," *Applied Surface Science*, vol. 257, no. 24, pp. 10590–10594, 2011.

[6] K. Rokosz and T. Hryniewicz, "Characteristics of porous biocompatible coatings obtained on Niobium and Titanium-Niobium-Zirconium (TNZ) alloy by Plasma Electrolytic Oxidation," *Mechanik*, vol. 12, pp. 15–18, 2015.

[7] A. Norlin, "Porous Niobium Oxide as Electrode Material and Manufacturing Process," US 20090292346 A1, 2005.

[8] A. Norlin, J. Pan, and C. Leygraf, "Fabrication of porous Nb_2O_5 by plasma electrolysis anodization and electrochemical characterization of the oxide," *Journal of the Electrochemical Society*, vol. 153, no. 7, pp. B225–B230, 2006.

[9] M. Sowa, A. Kazek-Kęsik, A. Krząkała et al., "Modification of niobium surfaces using plasma electrolytic oxidation in silicate solutions," *Journal of Solid State Electrochemistry*, vol. 18, no. 11, pp. 3129–3142, 2014.

[10] J. B. Bajat, V. Mišković-Stanković, R. Vasilić, and S. Stojadinović, "Corrosion evaluation of zirconium doped oxide coatings on aluminum formed by plasma electrolytic oxidation," *Acta Chimica Slovenica*, vol. 61, no. 2, pp. 308–315, 2014.

[11] Y. Chen, X. Nie, and D. O. Northwood, "Plasma electrolytic oxidation (PEO) coatings on a zirconium alloy for improved wear and corrosion resistance," in *Proceedings of the Nuclear Frontiers 30th Annual Canadian Nuclear Society Conference and 33rd CNS/CNA Student Conference*, p. 275, Canadian Nuclear Society, Alberta, Canada, 2009.

[12] W. Xue, Q. Zhu, Q. Jin, and M. Hua, "Characterization of ceramic coatings fabricated on zirconium alloy by plasma electrolytic oxidation in silicate electrolyte," *Materials Chemistry and Physics*, vol. 120, no. 2-3, pp. 656–660, 2010.

[13] E. Matykina, R. Arrabal, P. Skeldon, G. E. Thompson, P. Wang, and P. Wood, "Plasma electrolytic oxidation of a zirconium alloy under AC conditions," *Surface and Coatings Technology*, vol. 204, no. 14, pp. 2142–2151, 2010.

[14] S. V. Gnedenkov, Y. P. Sharkeev, S. L. Sinebryukhov et al., "Functional coatings formed on the titanium and magnesium alloys as implant materials by plasma electrolytic oxidation technology: fundamental principles and synthesis conditions," *Corrosion Reviews*, vol. 34, no. 1-2, pp. 65–83, 2016.

[15] Y. Han, S.-H. Hong, and K. Xu, "Synthesis of nanocrystalline titania films by micro-arc oxidation," *Materials Letters*, vol. 56, no. 5, pp. 744–747, 2002.

[16] T. H. Teh, A. Berkani, S. Mato et al., "Initial stages of plasma electrolytic oxidation of titanium," *Corrosion Science*, vol. 45, no. 12, pp. 2757–2768, 2003.

[17] C. Fei, Z. Hai, C. Chen, and X. Yangjian, "Study on the tribological performance of ceramic coatings on titanium alloy surfaces obtained through microarc oxidation," *Progress in Organic Coatings*, vol. 64, no. 2-3, pp. 264–267, 2009.

[18] K. Rokosz, T. Hryniewicz, and S. Raaen, "Development of plasma electrolytic oxidation for improved Ti6Al4V biomaterial surface properties," *The International Journal of Advanced Manufacturing Technology*, vol. 85, pp. 2425–2437, 2015.

[19] K. Rokosz, T. Hryniewicz, S. Raaen, and P. Chapon, "Investigation of porous coatings obtained on Ti-Nb-Zr-Sn alloy biomaterial by plasma electrolytic oxidation: characterisation and modelling," *The International Journal of Advanced Manufacturing Technology*, vol. 87, no. 9, pp. 3497–3512, 2016.

[20] W. Simka, A. Iwaniak, G. Nawrat et al., "Modification of titanium oxide layer by calcium and phosphorus," *Electrochimica Acta*, vol. 54, no. 27, pp. 6983–6988, 2009.

[21] K. Rokosz, T. Hryniewicz, Ł. Dudek, D. Matýsek, J. Valíček, and M. Harničárová, "SEM and EDS analysis of surface layer formed on titanium after plasma electrolytic oxidation in H_3PO_4 with the addition of $Cu(NO_3)_2$," *Journal of Nanoscience and Nanotechnology*, vol. 16, no. 8, pp. 7814–7817, 2016.

[22] Z. Yao, Y. Jiang, F. Jia, Z. Jiang, and F. Wang, "Growth characteristics of plasma electrolytic oxidation ceramic coatings on Ti-6Al-4V alloy," *Applied Surface Science*, vol. 254, no. 13, pp. 4084–4091, 2008.

[23] R. O. Hussein, X. Nie, and D. O. Northwood, "A spectroscopic and microstructural study of oxide coatings produced on a Ti-6Al-4V alloy by plasma electrolytic oxidation," *Materials Chemistry and Physics*, vol. 134, no. 1, pp. 484–492, 2012.

[24] A. Krząkala, J. Młyński, G. Dercz et al., "Modification of Ti 6Al-4V alloy surface by EPD-PEO process in ZrSiO4 suspension," *Archives of Metallurgy and Materials*, vol. 59, no. 1, pp. 199–204, 2014.

[25] X. Zhang, X. Huang, Y. Ma, N. Lin, A. Fan, and B. Tang, "Bactericidal behavior of Cu-containing stainless steel surfaces," *Applied Surface Science*, vol. 258, no. 24, pp. 10058–10063, 2012.

[26] Casa Software Ltd, CasaXPS: Processing Software for XPS, AES, SIMS and More, 2009, http://www.casaxps.com.

[27] X. Yao, X. Zhang, H. Wu, L. Tian, Y. Ma, and B. Tang, "Microstructure and antibacterial properties of Cu-doped TiO_2 coating on titanium by micro-arc oxidation," *Applied Surface Science*, vol. 292, pp. 944–947, 2014.

[28] C. D. Wagner, A. V. Naumkin, A. Kraut-Vass, J. W. Allison, C. J. Powell, and J. R. Rumble Jr., *NIST Standard Reference Database 20, Version 3.4*, 2003, http://srdata.nist.gov/xps.

[29] F. Hempel, B. Finke, C. Zietz, R. Bader, K.-D. Weltmann, and M. Polak, "Antimicrobial surface modification of titanium substrates by means of plasma immersion ion implantation and deposition of copper," *Surface and Coatings Technology*, vol. 256, pp. 52–58, 2014.

[30] J. Morales, J. P. Espinos, A. Caballero, and A. R. Gonzalez-Elipe, "XPS study of interface and ligand effects in supported Cu_2O and CuO nanometric particles," *The Journal of Physical Chemistry B*, vol. 109, no. 16, pp. 7758–7765, 2005.

[31] W. Zhu, Z. Zhang, B. Gu, J. Sun, and L. Zhu, "Biological activity and antibacterial property of nano-structured TiO_2 coating incorporated with Cu prepared by micro-arc oxidation," *Journal of Materials Science & Technology*, vol. 29, no. 3, pp. 237–244, 2013.

[32] A. J. Marenco, D. B. Pedersen, and S. Trudel, "Inducing ferromagnetic behavior in Cu nanoparticles and thin films through nonstoichiometric oxidation," *The Journal of Physical Chemistry C*, vol. 120, no. 13, pp. 7388–7396, 2016.

[33] A. Yin, X. Guo, W.-L. Dai, and K. Fan, "The nature of active copper species in Cu-HMS catalyst for hydrogenation of dimethyl oxalate to ethylene glycol: new insights on the synergetic effect between Cu^0 and Cu^+," *The Journal of Physical Chemistry C*, vol. 113, no. 25, pp. 11003–11013, 2009.

[34] Pulsed RF Glow Discharge Optical Emission Spectrometry—Ultra Fast Elemental Depth Profiling, HORIBA Scientific, Printed in France—©HORIBA Jobin Yvon: 7 pages, 2014, http://www.horiba.com/scientific/products/atomic-emission-spectroscopy/glow-discharge/.

[35] J. Kolmas, E. Groszyk, and D. Kwiatkowska-Rózycka, "Substituted hydroxyapatites with antibacterial properties," *BioMed Research International*, vol. 2014, Article ID 178123, 15 pages, 2014.

International Journal of
Medicinal Chemistry

Organic Chemistry
International

International Journal of
Photoenergy

International Journal of
Analytical Chemistry

Advances in
Physical Chemistry

International Journal of
Carbohydrate
Chemistry

Journal of
Quantum Chemistry

The Scientific
World Journal

Journal of
Analytical Methods
in Chemistry

Journal of
Spectroscopy

International Journal of
Inorganic Chemistry

International Journal of
Electrochemistry

Journal of
Applied Chemistry

Bioinorganic Chemistry
and Applications

Hindawi

Submit your manuscripts at
http://www.hindawi.com

Journal of
Theoretical Chemistry

Chromatography
Research International

Journal of
Catalysts

Journal of
Chemistry

International Journal of
Spectroscopy